SCIENCE CHINA Materials ARTICLES

mater.scichina.com link.springer.com

Published online 28 November 2017 | https://doi.org/10.1007/s40843-017-9130-x

Sci China Mater 2018, 61(1): 65–72

Electron transport layer driven to improve the open-circuit voltage of $CH_3NH_3PbI_3$ planar perovskite solar cells

Xin Yao[1,2,3,4], Junhui Liang[1,2,3,4], Tiantian Li[1,2,3,4], Lin Fan[1,2,3,4], Biao Shi[1,2,3,4], Changchun Wei[1,2,3,4], Yi Ding[1,2,3,4], Yuelong Li[1,2,3,4], Ying Zhao[1,2,3,4] and Xiaodan Zhang[1,2,3,4*]

ABSTRACT **Suitable electron transport layers are essential for high performance planar perovskite heterojunction solar cells. Here, we use ZnO electron transport layer sputtered under oxygen-rich atmosphere at room temperature to decrease the hydroxide and then suppress decomposition of perovskite films. The perovskite films with improved crystallinity and morphology are achieved. Besides, on the ZnO substrate fabricated at oxygen-rich atmosphere, open-circuit voltage of the $CH_3NH_3PbI_3$-based perovskite solar cells increased by 0.13 V. A high open-circuit voltage of 1.16 V provides a good prospect for the perovskite-based tandem solar cells. The ZnO sputtered at room temperature can be easily fabricated industrially on a large scale, therefore, compatible to flexible and tandem devices. Those properties make the sputtered ZnO films promising as electron transport materials for perovskite solar cells.**

Keywords: planar perovskite solar cells, electron transport layer, hydroxide, suppressed decomposition process, enhanced crystallization and morphology

INTRODUCTION

Perovskite solar cells based on an organolead halide light harvester have triggered worldwide intense concentrations due to their advantages of meteoric rise in power conversion efficiencies, low-cost precursor materials and simple preparation technology. Over the past eight years, the efficiency of perovskite solar cells has a stunning growth from 3.8% [1] to over 22% [2].

There are two main categories in perovskite solar cells (PSCs), mesoscopic [3–8] and planar [9–14] structure. As the planar device has a simpler fabrication process and avoids the high temperature treatment of mesoporous scaffold, substantial efforts have been made on the planar PSCs to obtain an exceptional performance. In the commonly used N-I-P type planar perovskite solar cell structures, perovskite absorber deposited directly on the electron transport layer (ETL). Besides, the excitons, generated in perovskite layer, separate at the interface and diffuse directly to the ETL. Therefore, the ETL in N-I-P type planar structure is essential for the crystallization and morphology of perovskite films [15,16] and used to extract electrons [17–19]. Until now, TiO_2 is the most widely used ETL in perovskite solar cells [20–22]; however, ZnO has a higher carrier mobility, conductivity and a similar energy band profile with TiO_2, ensuring a faster electron transport. Moreover, good electrical conductivity [23] can guarantee even in the deposition process at room temperature. Therefore, as a good alternative, ZnO can be widely applied as a promising electron transport material for perovskite solar cells, which is also compatible to flexible and tandem devices.

ZnO has been successfully assembled in perovskite solar cells, and usually deposited through chemical methods, such as immersion [24], sol-gel method [25], electro-deposition [26], hydrothermal route [27]. These chemical processes mold different morphologies at nanoscale, e.g., nanorods [28] and nanoparticles [29], with a better infiltration and absorption for perovskite films. Nevertheless, to further simplify these chemical approaches for large-scale film fabrication, a few advanced deposition techniques have been developed, for instance,

[1] Institute of Photoelectronic Thin Film Devices and Technology of Nankai University, Tianjin 300071, China
[2] Key Laboratory of Photoelectronic Thin Film Devices and Technology of Tianjin, Tianjin 300071, China
[3] Key Laboratory of Optical Information Science and Technology of Ministry of Education, Tianjin 300071, China
[4] Collaborative Innovation Center of Chemical Science and Engineering (Tianjin), Tianjin 300072, China
* Corresponding author (email: xdzhang@nankai.edu.cn)

the plasma-enhanced chemical vapor deposition (PECVD) [30] and sputtered method [31]. However, all the perovskite films fabricated on ZnO substrate have a low annealing temperature and short annealing time, as the hydroxide in ZnO can accelerate the decomposition of the perovskite films. As a result, the perovskite crystal growth and the photovoltaic performance are limited. To relieve the decomposition, poly(ethylenimine) [32] and Al_2O_3 [33] buffer layer have been adopted to prevent from the direct contact of ZnO and perovskite. Therefore, hydroxide could not participate in the decomposition.

Here, ZnO films are sputtered as the ETL in perovskite solar cells. The sputtered films are uniform, compact, and can be available in industrial production. Moreover, the films can be fabricated even at room temperature. Therefore, they are compatible to thermal-sensitive devices, such as flexible and tandem devices. Furthermore, in this work, we have found that the ZnO films prepared under oxygen-rich atmosphere could effectively reduce the concentration of hydroxide, and then suppress the decomposition of perovskite films, consequently promoting their crystallization and morphology.

EXPERIMENTAL SECTION

Materials

Methylammonium iodide (CH_3NH_3I) was purchased from Shanghai MaterWin New Materials Corporation and lead chloride ($PbCl_2$), lead iodide (PbI_2) were purchased from Sigma-Aldrich and used without further purication. Anhydrous dimethylsulfoxide (DMSO) and 2-propanol were purchased from Tianjin Guangfu Fine Chemical Research Institute. The organic hole transporting material, spiro-OMeTAD (2,2',7,7'-tetrakis (*N*,*N*-di-*p*-methoxy-phenylamine)-9,9'-spirobifluorene) (≥99.0%) was purchased from Shenzhen Feiming Science and Technology Co., Ltd. Lithium-*bis*(trifluoromethane) sulfonyl imide (Li-TFSI) and 4-tertbutylpyridine (TBP) were purchased from Aladdin Reagents. A transparent conducting fluorine-doped SnO_2-coated glass substrate (FTO) was ultrasonically rinsed sequentially in detergent, deionized water and flnally dried under a flow of clean air.

Device fabrication

ZnO films were deposited on the FTO substrate using pulsed direct-current magnetron sputtering system. Intrinsic ZnO ceramic target (99.999%) was selected and oxygen flow rate varied from 0 to 20 sccm. Substrate was kept at room temperature. ZnO film thickness was kept as a constant of 75 nm.

A 1 mol L^{-1} perovskite precursor solution was prepared from $PbCl_2$ and PbI_2 with 1:1 molar ratio in DMSO and spin-coated onto the ZnO films at 3,000 rpm with the solution at 70°C. The films were then dipped in a solution of CH_3NH_3I in 2-propanol (10 mg mL^{-1}) for 10 min in the ambient atmosphere, and rinsed with 2-propanol. After drying, the samples were annealed at 70°C for 10 min. Hole transport layer (HTL) was deposited subsequently by spin coating of HTL solution at 5,000 rpm. The HTL solution consists of 80 mg spiro-OMeTAD, 28.5 μL 4-tertbutylpyridine and 17.5 μL Li-TFSI solution (520 mg in 1 mL acetonitrile), dissolved in 1 mL chlorobenzene. Finally, a 100-nm thick Au layer was deposited on the HTL layer by thermal evaporation. All those processes were completed in the atmosphere.

Characterization

Crystal structure of the perovskite films was examined by X-ray diffraction (XRD) spectra (a Rigaku, ATX-XRD) with Cu Kα radiation (λ=1.5405 Å) in the 2θ range from 3° to 80°. The transmission and absorption spectra were recorded with a Varian Cary 5000 UV-visible-NIR spectrophotometer in the wavelength ranging from 300 to 800 nm. The morphologies of perovskite thin films were observed using a scanning electron microscope (SEM) (Jeol JSM-6700F). Grain sizes distribution was estimated from the SEM images using Nano measurer 1.2 software. The size of each grain was measured and then calculated to obtain the average size in each SEM image. Surface morphology of films was revealed using atomic force microscopy (AFM, NanoNavi-SPA400). The active area of the perovskite solar cells was 0.1 cm^2. The photocurrent density-voltage (*J*-*V*) curves of the solar cells were measured at 25°C under AM 1.5 (100 mW cm^{-2}) light illumination. The oxygen vacancy and O 1s core peak of film were investigated using X-ray photoelectron spectroscopy (XPS, PHI5000VersaProbe). The spectral response was taken by an external quantum efficiency (EQE) measurement system (QEX10, PV Measurement).

RESULTS AND DISCUSSION

Planar perovskite solar cells were fabricated using ZnO films as ETL which plays a vital role in determining performance of PSC as it has a direct influence on the crystallization and morphology of perovskite films. We speculate that ZnO is not completely oxidized during the synthesis process, and then the generated hydroxide (OH^-) can break the ionic interaction between $CH_3NH_3^+$ and PbI_3^- and eventually collapse the crystal structure of

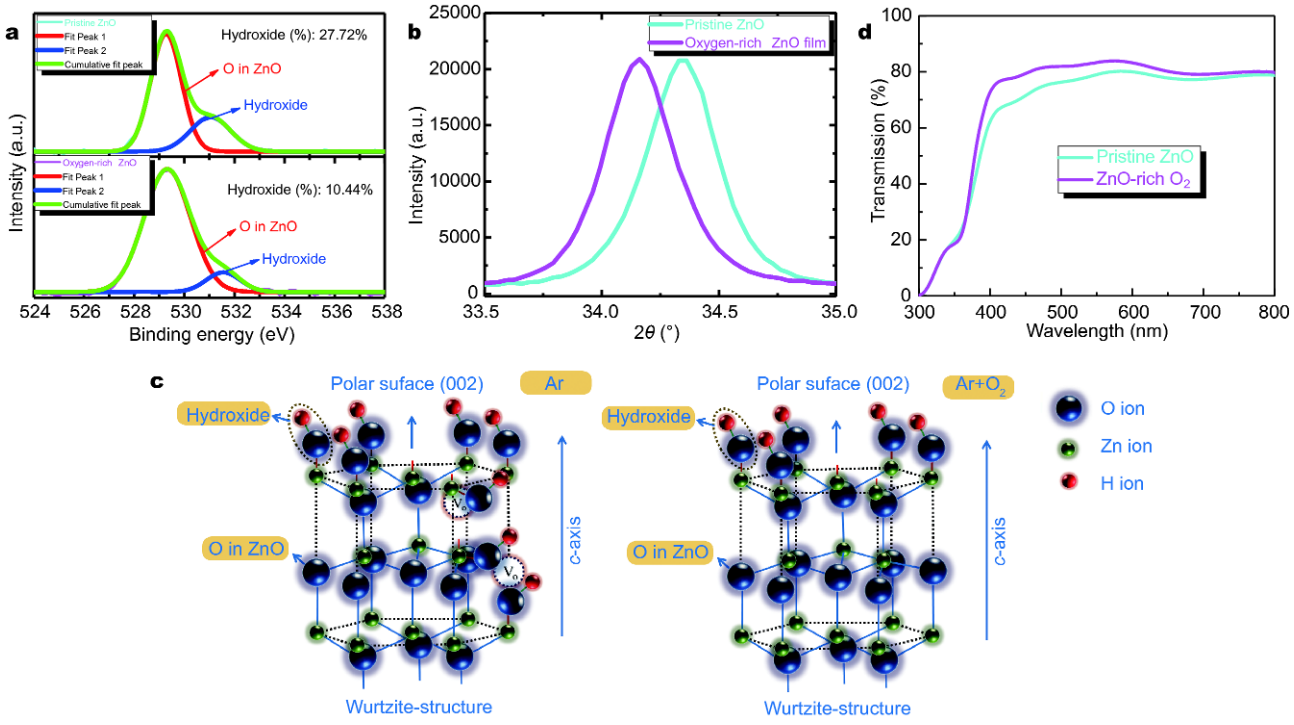

Figure 1 Features of the pristine ZnO and oxygen-rich ZnO film: (a) high-resolution of O 1s XPS core level spectra. (b) XRD pattern. (c) Wurtzite structure. (d) Transmittance spectra.

Table 1 2θ and FWHM data analyzed from XRD pattern

Sample	Pristine ZnO	Oxygen-rich ZnO
2θ	34.34	34.16
FWHM	0.392	0.376

perovskite. As described in Equations (1–3), OH^- reacts with CH_3NH_3I and forms CH_3NH_3OH. The CH_3NH_3OH would then easily decompose to CH_3NH_2 and H_2O during the annealing process, consequently with an accelerating decomposition of perovskite films. We expect that the oxygen-rich environment will suppress the formation of hydroxide and promote the crystallization of perovskite films.

$$CH_3NH_3I + PbI_2 \rightleftharpoons CH_3NH_3PbI_3 \quad (1)$$

$$OH^- + CH_3NH_3I \rightarrow CH_3NH_3OH + I^- \quad (2)$$

$$CH_3NH_3OH \xrightarrow{heat} CH_3NH_2\uparrow + H_2O\uparrow \quad (3)$$

Oxygen (O) 1s core level XPS spectrum has been employed to obtain the information about the hydroxide in ZnO ETL. Fig. 1a shows the O 1s core level spectra for the as-prepared ZnO films without oxygen environment (pristine ZnO) and with oxygen flow rate of 15 sccm (oxygen-rich ZnO), respectively. It is noted that all the samples are handled in the same way for data collection. O 1s peak shows a slightly asymmetric shape, which can be deconvoluted carefully into two Gaussian peaks located at 528.7 and 530.4 eV, orresponding to the O 1s level and hydroxide in ZnO, respectively [32]. Accordingly, the decrease of peak area ratio (concentration of hydroxide) in the oxygen-rich environment indicates that the hydroxide in ZnO is suppressed. The crystal structure of ZnO films was investigated with XRD, as depicted in Fig. 1b. The (002) diffraction peak angle (2θ) shifted to left indicates a larger lattice constant and the concentration of oxygen vacancy decreases in oxygen-rich environment, with reduced recombination loss in solar cells, further improving the open-circuit voltage (V_{OC}). Furthermore, the full width at half-maximum (FWHM) of the oriented peak decreases slightly in the oxygen-rich environment. The decrease in FWHM corresponds to the increase in grain size with a higher mobility, which is beneficial to the carrier transport. The schematic diagram of ZnO microstructures fabricated with and without oxygen environment is presented in Fig. 1c. Fig. 1d reveals the optical transmission spectra of ZnO films. A higher transmittance in the wavelength range of 400–600 nm is obtained with oxygen-rich environment, allowing more photo flux to reach the absorber layer for photon-generated carriers.

The pristine ZnO and oxygen-rich ZnO films are ap-

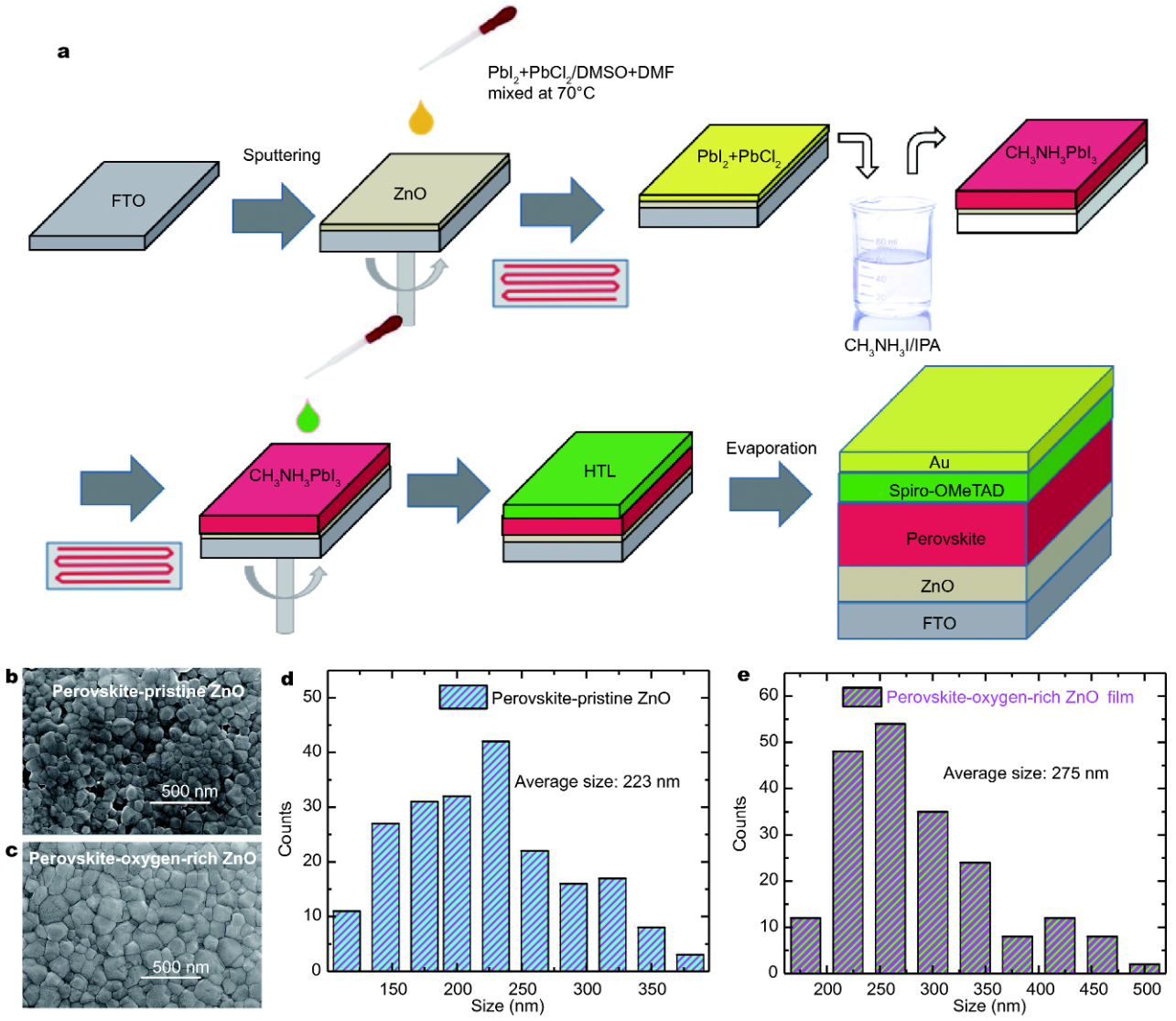

Figure 2 (a) Schematic descriptions of the device fabrication process. (b, c) Top-view SEM images of perovskite films based on pristine ZnO and oxygen-rich ZnO respectively. (d, e) Grain size distributions as estimated from the SEM images using Nano measurer 1.2 software.

plied to planar PSC devices, whose fabrication processes are schematically depicted in Fig. 2a, adapted from a previous report [34]. To further characterize the function of ZnO ETL fabricated with different atmosphere, surface morphology of perovskite films deposited on ZnO substrate is examined through top-view SEM images, as shown in Fig. 2b, c. With the oxygen-rich environment, uniform and flat perovskite films have been achieved, eliminating pin-holes generated in the pristine ZnO substrate, with crystalline features on the length scale of hundreds of nanometers. Besides, the close inspection of the surface images shows a larger grain size of perovskite layer with an average crystal size increasing from 223 to 275 nm (see statistical distribution in Fig. 2d, e). The ameliorated morphology stems from the suppressed hydroxide in ZnO films. The larger grain size and reduced grain boundaries are beneficial to an increased short circuit current density (J_{SC}).

The absorption spectra of the perovskite films prepared on different ZnO substrates are presented in Fig. 3a. As depicted, the absorbance of the perovskite films increases in oxygen rich environment. This is partly due to the slightly as-increased transmission of ZnO films and better morphology of perovskite films. The improved crystallinity as discussed in the following may also be responsible for it. Fig. 3b shows the crystalline structures of

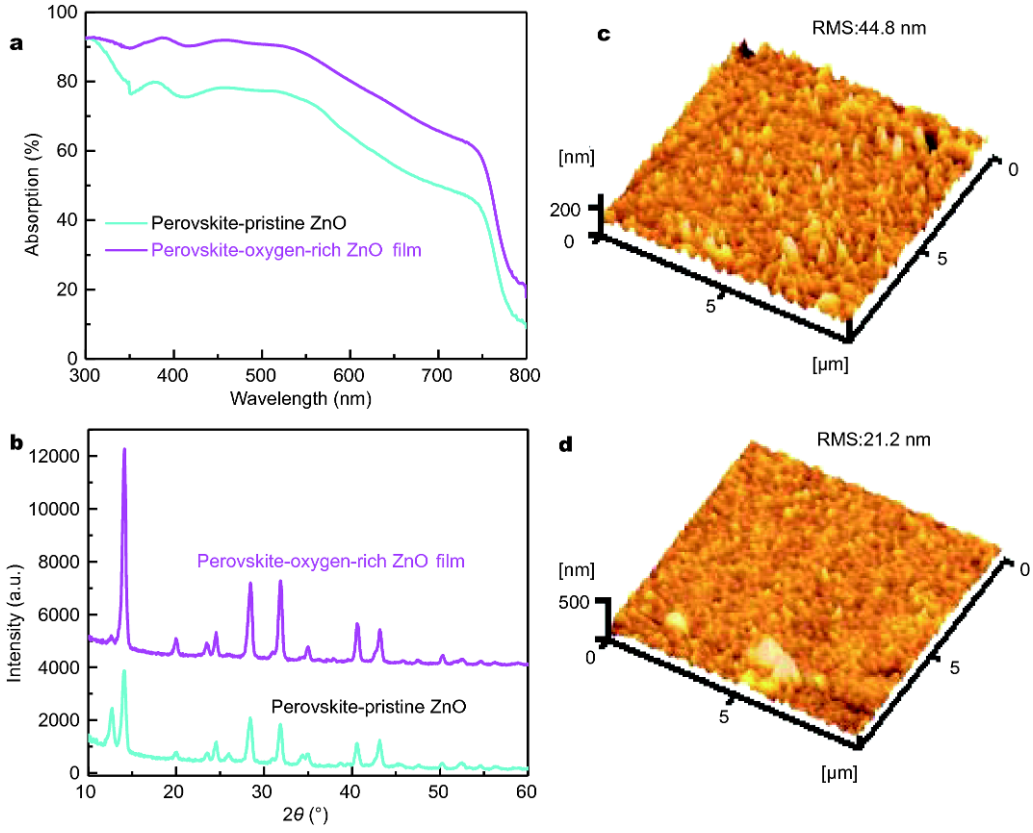

Figure 3 Perovskite films deposited on ZnO in different atmosphere: (a) absorption spectra. (b) XRD pattern. (c and d) AFM images of perovskite films on pristine ZnO and oxygen-rich ZnO substrate, respectively.

perovskite films based on ZnO substrates. The peaks at 2θ=14.2°, 28.6°, 31.8°, 40.7° and 43.2° correspond to $CH_3NH_3PbI_3$ (110), (220), (310), (224) and (314) orientation, respectively, which is consistent with the previously reported data of $CH_3NH_3PbI_3$ crystallized in the tetragonal perovskite structure [35]. Moreover, the strongest (110) diffraction peak indicates a preferential growth direction along the (110) direction. The stronger diffraction peaks of the perovskite films with oxygen-rich environment indicate the better crystalline quality of perovskite. In addition, for the pristine ZnO substrate, the peak 2θ=12.8° of PbI_2 implies the decomposition of perovskite films. Nevertheless, impurity phase can be hardly seen in the XRD pattern based on oxygen-rich ZnO films, indicating a high-level purities and the suppressed decomposition process. AFM images are obtained to further characterize the surface morphology of perovskite films, as shown in Fig. 3c, d. The AFM images illustrate a decreased roughness with oxygen-rich environment, with the root-mean-square (RMS) roughness decreasing from 44.8 to 21.2 nm, indicating a flatter perovskite surface is favorable for deposition of following hole transport layer on the top and provides a more sufficient contact between both layers.

As illustrated above, the oxygen-rich environment is beneficial to the subsequent spin-coating process of perovskite films with an improved morphology and crystallization. We have applied ZnO substrates to perovskite solar cells with different oxygen flow rates at 0, 5, 10, 15 and 20 sccm. The statistical values and best *J-V* curves of different oxygen flow rates are demonstrated in Fig. 4a, b, respectively. The detailed photovoltaic parameters of these devices are given in Table 2. A continuous improvement of V_{OC} and fill factor (FF) can be observed with increasing oxygen flow rate, while the J_{SC} and efficiency present their maximum value at 15 sccm. The increased V_{OC} partly results from the passivated hydroxide and oxygen vacancies, which can suppress the carrier recombination in ZnO ETL. Furthermore, the enhanced crystallinity and ameliorated morphology of the perovskite films also suppress the recombination, leading to a high V_{OC}. The improvement of J_{SC} can be explained as

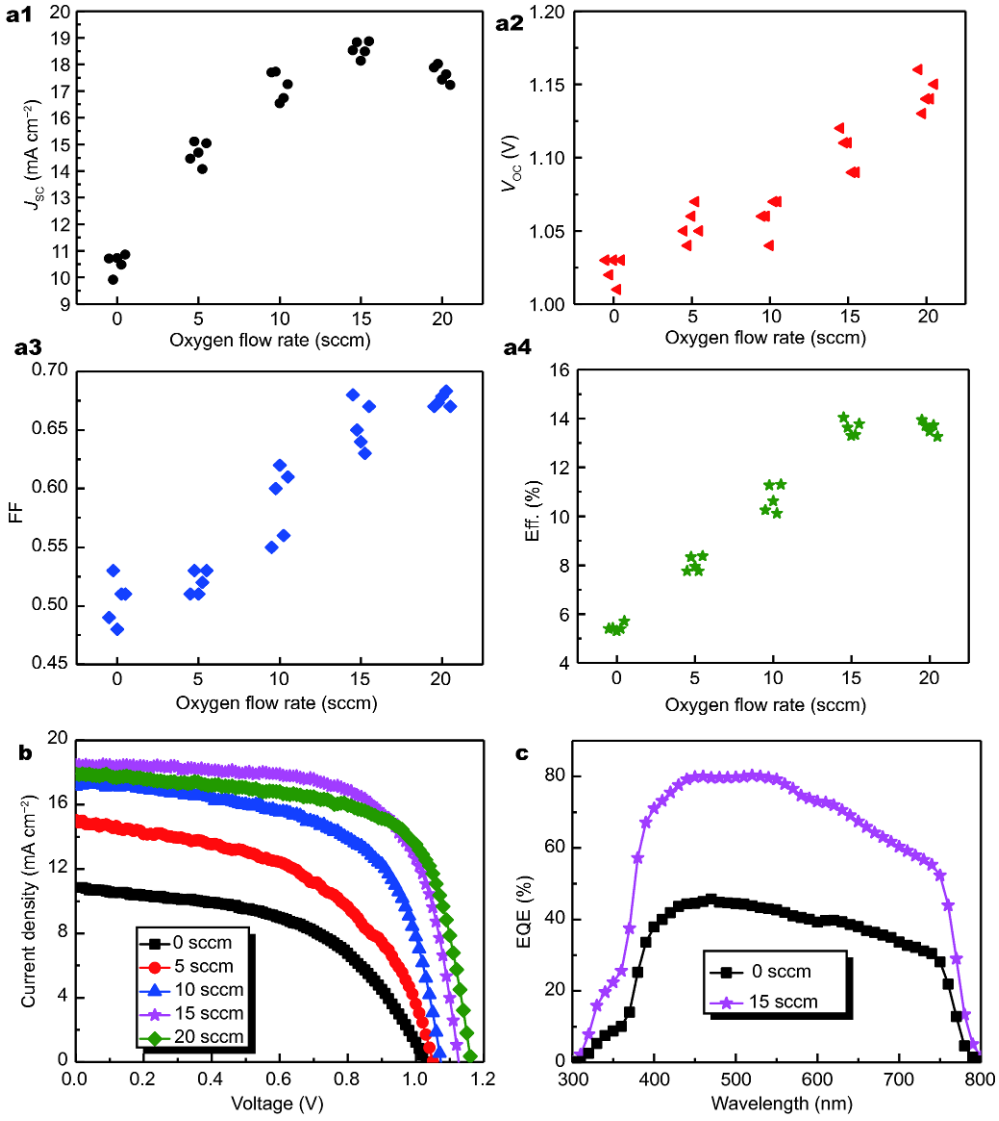

Figure 4 (a1–a4) Performances of the devices on ZnO substrates fabricated with different oxygen flow rates. (b) Photocurrent-voltage curves of the best-performing perovskite solar cell based on ZnO films with different oxygen flow rate measured under simulated AM 1.5 sunlight of 100 mW cm^{-2} irradiance. (c) EQE spectra of perovskite solar cells based on ZnO films with oxygen flow rate of 0 and 15 sccm.

Table 2 Performance parameters of solar cells based on different ETLs

Samples	V_{OC} (V)	J_{SC} (mA cm^{-2})	FF	PCE (%)	R_{SH} (Ω cm^2)	R_S (Ω cm^2)
0 sccm	1.03	10.86	0.51	5.70	516	25.08
5 sccm	1.05	15.04	0.53	8.37	628	10.98
10 sccm	1.07	17.25	0.61	11.30	861	7.37
15 sccm	1.12	18.53	0.68	14.04	1852	6.25
20 sccm	1.16	17.88	0.67	13.94	1953	6.63

follows: (1) the absorbance of the perovskite films is enhanced; (2) the better crystalline quality of perovskite and the larger grains; (3) the flatter perovskite films enable more sufficient contact of perovskite films with the HTL, which is beneficial to the carrier transport. When the oxygen flow rate was up to 20 sccm, there is a slight decrease in J_{SC}. The reason may be the increased vertical resistivity of ZnO as a barrier for carrier transportation,

resulting in a lower carrier collection rate. The EQE curves for perovskite solar cells with oxygen flow rate of 0 (pristine ZnO) and 15 sccm (oxygen-rich ZnO) are illustrated in Fig. 4c. We can observe an increase of the current in the oxygen-rich environment in the *J-V* curves. The perovskite solar cell based on ZnO ETL shows the best PCE with oxygen flow rate of 15 sccm, and the V_{OC}, J_{SC}, FF and PCE are 1.12 V, 18.53 mA cm^{-2}, 0.68 and 14.04%, respectively.

CONCLUSIONS

In summary, we have reported an efficient method to suppress the decomposition of perovskite films induced by the hydroxide in ZnO ETL sputtered under oxygen-rich environment, which can effectively passivate the hydroxide and oxygen vacancy in ZnO to reduce the defect densities as well. With the improved crystallinity of perovskite films, the ZnO sputtered in oxygen-rich environment also contributes to a stronger absorption and flatter perovskite film and thus promotes the J_{SC} of solar cells. These effects lead to values of V_{OC} as high as 1.16 V for $CH_3NH_3PbI_3$-based perovskite solar cells. These combinations of ease-of-fabrication, high V_{OC}, room-temperature and industrial large-scale processing are all expected to push the hybrid organic–inorganic solar cells compatible to flexible and tandem devices and closer to commercial viability.

Received 19 July 2017; accepted 18 September 2017; published online 28 November 2017

1 Kojima A, Teshima K, Shirai Y, *et al.* Organometal halide perovskites as visible-light sensitizers for photovoltaic cells. J Am Chem Soc, 2009, 131: 6050–6051
2 Nrel efficiency chart. https://www.nrel.gov/pv/assets/images/efficiency-chart.png
3 Lv S, Han L, Xiao J, *et al.* Mesoscopic TiO_2/$CH_3NH_3PbI_3$ perovskite solar cells with new hole-transporting materials containing butadiene derivatives. Chem Commun, 2014, 50: 6931–6934
4 Pang S, Hu H, Zhang J, *et al.* $NH_2CHNH_2PbI_3$: an alternative organolead iodide perovskite sensitizer for mesoscopic solar cells. Chem Mater, 2014, 26: 1485–1491
5 Kim HS, Lee CR, Im JH, *et al.* Lead iodide perovskite sensitized all-solid-state submicron thin film mesoscopic solar cell with efficiency exceeding 9%. Sci Rep, 2012, 2: 591
6 Mei A, Li X, Liu L, *et al.* A hole-conductor-free, fully printable mesoscopic perovskite solar cell with high stability. Science, 2014, 345: 295–298
7 Malinkiewicz O, Yella A, Lee YH, *et al.* Perovskite solar cells employing organic charge-transport layers. Nat Photon, 2014, 8: 128–132
8 Jeon NJ, Noh JH, Kim YC, *et al.* Solvent engineering for high-performance inorganic–organic hybrid perovskite solar cells. Nat Mater, 2014, 13: 897–903
9 Hou Y, Quiroz COR, Scheiner S, *et al.* Low-temperature and hysteresis-free electron-transporting layers for efficient, regular, and planar structure perovskite solar cells. Adv Energ Mater, 2015, 5: 1501056
10 Wu H, Zhang C, Ding K, *et al.* Efficient planar heterojunction perovskite solar cells fabricated by *in-situ* thermal-annealing doctor blading in ambient condition. Org Electron, 2017, 45: 302–307
11 Wang C, Yang J. Interface modification for organic and perovskite solar cells. Sci China Mater, 2016, 59: 743–756
12 Eperon GE, Stranks SD, Menelaou C, *et al.* Formamidinium lead trihalide: a broadly tunable perovskite for efficient planar heterojunction solar cells. Energ Environ Sci, 2014, 7: 982–988
13 Wu Y, Islam A, Yang X, *et al.* Retarding the crystallization of PbI_2 for highly reproducible planar-structured perovskite solar cells *via* sequential deposition. Energ Environ Sci, 2014, 7: 2934–2938
14 Liu M, Johnston MB, Snaith HJ. Efficient planar heterojunction perovskite solar cells by vapour deposition. Nature, 2013, 501: 395–398
15 Bera A, Sheikh AD, Haque MA, *et al.* Fast crystallization and improved stability of perovskite solar cells with Zn_2SnO_4 electron transporting layer: interface matters. ACS Appl Mater Interfaces, 2015, 7: 28404–28411
16 Fu F, Feurer T, Jäger T, *et al.* Low-temperature-processed efficient semi-transparent planar perovskite solar cells for bifacial and tandem applications. Nat Commun, 2015, 6: 8932
17 Jiang Q, Zhang L, Wang H, *et al.* Enhanced electron extraction using SnO_2 for high-efficiency planar-structure $HC(NH_2)_2PbI_3$-based perovskite solar cells. Nat Energ, 2016, 2: 16177
18 Ren X, Yang D, Yang Z, *et al.* Solution-processed Nb:SnO_2 electron transport layer for efficient planar perovskite solar cells. ACS Appl Mater Interfaces, 2017, 9: 2421–2429
19 Chen BX, Rao HS, Li WG, *et al.* Achieving high-performance planar perovskite solar cell with Nb-doped TiO_2 compact layer by enhanced electron injection and efficient charge extraction. J Mater Chem A, 2016, 4: 5647–5653
20 Yang D, Yang R, Zhang J, *et al.* High efficiency flexible perovskite solar cells using superior low temperature TiO_2. Energ Environ Sci, 2015, 8: 3208–3214
21 Zhou H, Chen Q, Li G, *et al.* Interface engineering of highly efficient perovskite solar cells. Science, 2014, 345: 542–546
22 Wang J, Qin M, Tao H, *et al.* Performance enhancement of perovskite solar cells with Mg-doped TiO_2 compact film as the hole-blocking layer. Appl Phys Lett, 2015, 106: 121104
23 Zhang C, Luo Q, Wu H, *et al.* Roll-to-roll micro-gravure printed large-area zinc oxide thin film as the electron transport layer for solution-processed polymer solar cells. Org Electron, 2017, 45: 190–197
24 Bi D, Boschloo G, Schwarzmüller S, *et al.* Efficient and stable $CH_3NH_3PbI_3$-sensitized ZnO nanorod array solid-state solar cells. Nanoscale, 2013, 5: 11686–11691
25 Dong J, Zhao Y, Shi J, *et al.* Impressive enhancement in the cell performance of ZnO nanorod-based perovskite solar cells with Al-doped ZnO interfacial modification. Chem Commun, 2014, 50: 13381–13384
26 Zhang J, Barboux P, Pauporté T. Electrochemical design of nanostructured ZnO charge carrier layers for efficient solid-state perovskite-sensitized solar cells. Adv Energ Mater, 2014, 4: 1400932
27 Dong J, Shi J, Li D, *et al.* Controlling the conduction band offset

for highly efficient ZnO nanorods based perovskite solar cell. Appl Phys Lett, 2015, 107: 073507
28 Son DY, Im JH, Kim HS, *et al.* 11% Efficient perovskite solar cell based on ZnO nanorods: an effective charge collection system. J Phys Chem C, 2014, 118: 16567–16573
29 Liu D, Kelly TL. Perovskite solar cells with a planar heterojunction structure prepared using room-temperature solution processing techniques. Nat Photon, 2014, 8: 133–138
30 Ramos FJ, López-Santos MC, Guillén E, *et al.* Perovskite solar cells based on nanocolumnar plasma-deposited ZnO thin films. ChemPhysChem, 2014, 15: 1148–1153
31 Liang L, Huang Z, Cai L, *et al.* Magnetron sputtered zinc oxide nanorods as thickness-insensitive cathode interlayer for perovskite planar-heterojunction solar cells. ACS Appl Mater Interfaces, 2014, 6: 20585–20589
32 Cheng Y, Yang QD, Xiao J, *et al.* Decomposition of organometal halide perovskite films on zinc oxide nanoparticles. ACS Appl Mater Interfaces, 2015, 7: 19986–19993
33 Song J, Zheng E, Wang XF, *et al.* Low-temperature-processed ZnO–SnO_2 nanocomposite for efficient planar perovskite solar cells. Sol Energ Mater Sol Cells, 2016, 144: 623–630
34 Burschka J, Pellet N, Moon SJ, *et al.* Sequential deposition as a route to high-performance perovskite-sensitized solar cells. Nature, 2013, 499: 316–319
35 Conings B, Baeten L, De Dobbelaere C, *et al.* Perovskite-based hybrid solar cells exceeding 10% efficiency with high reproducibility using a thin film sandwich approach. Adv Mater, 2014, 26: 2041–2046

Acknowledgements This work was supported by the International Cooperation Projects of the Ministry of Science and Technology (2014DFE60170), the National Natural Science Foundation of China (61474065 and 61674084), Tianjin Research Key Program of Application Foundation and Advanced Technology (15JCZDJC31300), the Key Project in the Science & Technology Pillar Program of Jiangsu Province (BE2014147-3), and the 111 Project (B16027).

Author contributions Zhang X conceived the study; Yao X and Liang J carried out the experiments; Yao X and Zhang X wrote the manuscript; Zhang X and Zhao Y supervised the project; all authors discussed the results and implications and commented on the manuscript at all stages.

Conflict of interest The authors declare that there is no conflict of interest.

Xin Yao is a PhD candidate of the College of Electronic Information and Optical Engineering at Nankai University. Her current interests include perovskite solar cells and perovskite/silicon tandem solar cells.

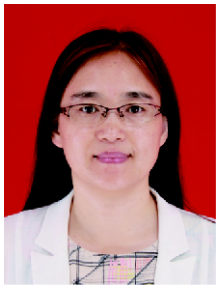

Xiaodan Zhang is the director of the Institute of Photoelectronic Thin Film Devices and Technology of Nankai University. Her research interests include the silicon and perovskite solar cells, optical/electro catalytic materials, plasma diagnostics and simulation.

电子传输层改善平面$CH_3NH_3PbI_3$钙钛矿太阳电池开路电压

姚鑫[1,2,3,4], 梁俊辉[1,2,3,4], 李天天[1,2,3,4], 范琳[1,2,3,4], 石标[1,2,3,4], 魏长春[1,2,3,4], 丁毅[1,2,3,4], 李跃龙[1,2,3,4], 赵颖[1,2,3,4], 张晓丹[1,2,3,4*]

摘要 电子传输层对于N-I-P型平面钙钛矿太阳电池的性能至关重要. ZnO薄膜由于其高载流子迁移率在钙钛矿太阳电池中被广泛应用, 但是薄膜内部羟基的存在影响了电池性能. 本文在磁控溅射沉积ZnO薄膜的过程中引入富氧环境来抑制ZnO中羟基的生成, 进而抑制钙钛矿薄膜的分解, 从而获得具有较高结晶质量的均匀致密的钙钛矿薄膜. 基于富氧环境下制备的ZnO作为电子传输层的钙钛矿太阳电池开压增加了0.13 V. 1.16 V的高开路电压对钙钛矿太阳电池在叠层电池中的应用提供了较好的发展前景. 此外, 室温磁控溅射制备的ZnO可以实现大面积工业化生产, 且适用于柔性和叠层器件. 该研究表明ZnO在太阳电池领域具有潜在应用.

